Chemical modifications of chitosan nano-based magnetic particles for enhanced uranyl sorption

Ahmed A. Galhoum, Mohammad G. Mahfouz, Nabawia M. Gomaa, Thierry Vincent, Eric Guibal

Chemical modifications of chitosan nano-based magnetic particles for enhanced uranyl sorption

Ahmed A. Galhoum [a,b], Mohammad G. Mahfouz [a], Nabawia M. Gomaa [a], Thierry Vincent [b], Eric Guibal [b,*]

[a] Nuclear Materials Authority, P.O. Box 530, Maadi, 11381 Cairo, Egypt
[b] Ecole des mines d'Alès, Centre des Matériaux des Mines d'Alès, 6 avenue de Clavières, F-30319 Alès cedex, France

A B S T R A C T

The grafting of diethylenetriamine (preferentially to the grafting of serine > cysteine > alanine) onto chitosan (immobilized on magnetic nano-based particles by combined polymer precipitation and hydrothermal treatment) allows synthesizing an efficient sorbent for uranyl at pH 4 (maximum sorption capacity close to 185 mg U g^{-1}). Sorption isotherm (regardless of the sorbent) is fitted by the Langmuir equation, while uptake kinetics is well described by the pseudo-second order rate equation. The design of nano-based particles (10–50 nm) allows reducing the impact of resistance to intraparticle diffusion on uptake kinetics and the equilibrium contact time is close to 45–60 min. The super paramagnetic properties of the hybrid materials make their solid/liquid separation quite easy using an external magnetic field. Finally uranyl ions can be desorbed using acidic urea solution (0.5 M, pH > 2) and the sorbents can be recycled for at least 5/6 cycles with a limited loss of sorption capacity (<9%).

Keywords:
Chitosan
Magnetic nano-based particles
Amino-acid grafting
Diethylene triamine
Uranyl
Sorption isotherm
Uptake kinetics
Metal desorption
Sorbent recycling

1. Introduction

Nano-based sorbents have recently received a great attention since decreasing the size of sorbent particles allows substantially reducing the limitations due to resistance to intraparticle diffusion and increasing specific surface area, which, in turn, improve uptake kinetics. These advantages are counter-balanced by the difficulty to manage these materials in batch systems and make impossible their use in continuous fixed-bed reactors. An alternative consists in supporting these active sorbents on a magnetic core and using an external magnetic field for recovering spent sorbents at the end of the sorption process (Chen et al., 2015; Zhou et al., 2014). These hybrid materials have significant advantages such as fast uptake kinetics and ready recovery of the materials for recycling and valorization of target metals. Obviously the cost of these materials is more expensive than standard sorbents; as a consequence their use is only competitive for the recovery of precious or strategic metals, for operating systems in hazardous environments (under irradiation for example) or for designing new materials (such as supported catalysts: immobilization of catalytic metal on an active layer deposited at the surface of magnetic core particles). The development of super magnets and electromagnetic systems has recently boosted this research field.

Two main processes have been described for the synthesis of these magnetic sorbents: (a) deposition of the active layer on pre-existing magnetic particles (magnetite powder), and (b) simultaneous conditioning of the active layer with the synthesis of magnetic nano-based objects. The simultaneous process of synthesis of magnetic particles and coating with active polymer layer allows generally producing smaller particles than the pure coating process. This is the main reason that made us selecting this procedure for the manufacturing of a series of hybrid magnetic materials based on functionalized chitosan. Chitosan was selected for its chemical compatibility with the synthesis procedure of preparation of magnetite particles. This is an amino-polysaccharide obtained by alkaline deacetylation of chitin (a renewable resource, characterized as poly-*N*-acetyl-D-glucosamine). Dissolved in acetic solution it can be mixed with magnetite precursors (i.e., ferric and ferrous salts) before being precipitated at controlled alkaline pH under heating to prepare magnetic chitosan-based nanoparticles. Chitosan is then entrapping magnetic nano-based particles. Chitosan has the intrinsic capacity of: (a) binding metal cations through chelation mechanisms on free amine groups in near neutral solutions (Guibal et al., 1995), and (b) sorbing metal anions in acidic solutions through electrostatic attraction/ion-exchange on protonated amine groups (Guibal, 2004). Depending on the pH of the metal solution it may be necessary cross-linking the biopolymer to prevent its dissolving and degradation. This

* Corresponding author.
E-mail addresses: galhoum_nma@yahoo.com (A.A. Galhoum), mahfouznma@yahoo.com (M.G. Mahfouz), g_nabawia@hotmail.com (N.M. Gomaa), thierry.vincent@mines-ales.fr (T. Vincent), eric.guibal@mines-ales.fr (E. Guibal).

post-treatment may have significant impact on metal sorption properties due to the loss of availability of amine groups (when they are involved in the cross-linking mechanism). For minimizing this loss of reactivity it may be useful grafting new functional groups on chitosan backbone (Elwakeel and Atia, 2014; Elwakeel et al., 2014; Xu et al., 2013; Yang et al., 2014). This chemical modification contributes not only to increase the density of sorption sites but also their selectivity (against pH, the composition of the solution, etc.) due to the specific reactivity of new functional groups: this makes these modified materials usable in much complex aqueous systems. In the present work are summarized a series of investigations performed using chitosan derivatives prepared by grafting amino-acids (cysteine, alanine, serine) and also amine-bearing compounds (diethylenetriamine). The physico-chemical properties of these materials were characterized using: VSM (magnetic properties), TEM (microscopic characterization), element analysis, FTIR spectroscopy, XRD spectrometry (Galhoum et al., 2015a, 2015b, 2015c, 2015e).

These materials were tested for uranium(VI) sorption, representative of toxic and valorizable metals ions (Donia et al., 2009), which can be found in nuclear industry, in mining effluents but also as a co-metal in some geological deposits that serve for phosphoric acid production and for recovery of rare earth metal ions (Lapidus and Doyle, 2015; Zagorodnyaya et al., 2013). The effect of pH on metal sorption is investigated, taking into account the stability of the sorbents. Sorption performance has been determined at pH 4, carrying out: (a) sorption isotherms at different temperatures for determination of maximum sorption capacities and thermodynamic parameters (Galhoum et al., 2015d; Mahfouz et al., 2015), (b) uptake kinetics (equilibrium contact time and diffusional regime), (c) metal desorption and resin recycling (life cycle of the sorbent).

2. Material & methods

2.1. Materials

Chitosan (90.5% deacetylation degree), diethylenetriamine (DETA, 98%), alanine, cysteine and serine amino acids, epichlorohydrin (EPI, >98%), were obtained from Sigma-Aldrich (France), 1,4-dioxane (99.9%) and ethanol were supplied by Fluka Chemicals (Switzerland). Arsenazo III (analytical grade reagent) was also obtained from Fluka Chemicals while all other chemicals were Prolabo products (used as received). Uranium stock solution was prepared from $UO_2(OCOCH_3)_2 \cdot 2H_2O$, supplied by Sigma-Aldrich, dissolved in concentrated sulfuric acid under heating and finally diluted in demineralized water (concentration: 1000 mg U L^{-1}). This sulfuric acid treatment was used to prepare solutions with a metal speciation similar to those obtained in the acidic leaching of Egyptian ores.

2.2. Synthesis of sorbents

The preferred method for the synthesis of the sorbents consisted in the co-synthesis of magnetic nano-based particles with the co-deposition of the biopolymer on magnetic cores (Galhoum et al., 2015a, 2015c). The principle of the synthesis of magnetite nano-objects is based on the Massart method (Massart, 1981): mixing of the precursors of magnetite (i.e., $FeSO_4$ and $FeCl_3$ salts with a molar ratio Fe(II)/Fe(III) = 1/2) and controlled precipitation followed by hydrothermal treatment. In the case of the synthesis of hybrid materials, the precursors were mixed together with 4 g of chitosan in 200 mL of an acetic acid solution (20% w/w). The pH was controlled to 10–10.5 using 2 M NaOH solution at 40 °C to precipitate the composite material (simultaneous synthesis of magnetite and precipitation of chitosan at the surface of magnetite micro-/nano-particles). Finally the precipitated material was matured by heating at 90 °C for 1 h under heating (with reflux). The particles were magnetically separated and abundantly rinsed in water. In a second step, the material was mixed (1:1 mass ratio) with an alkaline solution (pH close to 10) of epichlorohydrin (0.01 M in 0.067 M NaOH solution) under stirring at 40–50 °C for 2 h. This step contributes to stabilize the chitosan layer at the surface of magnetite particles. After magnetic separation and rinsing with demineralized water the sorbent was conditioning with epichlorohydrin in (1:1 v/v) ethanol/water mixture (15 mL EPI in 150 mL of solvent), prior to the grafting reaction with amino-acids or diethylenetriamine (in ethanol/water). Reaction took place at 75–80 °C overnight (for about 18 h). After magnetic separation and abundant rinsing the sorbent was finally freeze-dried. Fig. S1 (see Supplementary information) schematically represents the synthesis route. Magnetic separation was performed using "super-magnets" (NdFeB block magnets, www.supermagnete.fr) of different sizes depending on the amount of material to be separated. The separation is almost instantaneous (<5 s).

2.3. Characterization of sorbents

Amine concentration in the sorbent was characterized by alkaline titration on acidified suspension of sorbent (in HCl titrated solution). Fourier-Transform characterization of functional groups on the sorbents was performed on KBr discs using a Nexus 870 FTIR spectrometer (Nicolet, USA). Element analysis was performed on chitosan coated magnetic nano-based particles and on the sorbents using an automatic analyzer (CHNS Vario EL III elementar analyzer, Elementar, Germany). X-ray diffraction analysis was performed on granular form of sorbents at room temperature using a Philips X-ray generator model PW 3710/31 with the Cu K_α radiation in the range $2\theta = 10–90°$. A vibrating sample magnetometer (VSM, 730T, Lakeshoper, USA) was used for the magnetic characterization of sorbent samples; measurements were performed at room temperature. Atomic force microscopy and high resolution transmission electron microscopy were performed on WET-SPM Shimadzu (Japan) and HRTEM JEOL-2100 (Jeol, Japan).

2.4. Sorption studies

Sorption experiments were performed in agitated flasks by contact of a fixed amount of sorbent (m, g) with a volume of solution (V, L) containing a fixed concentration of uranium (C_0, mg L^{-1}) for 2 h. Indeed, preliminary experiments have confirmed that equilibrium time did not exceed 1 h. Agitation speed was set to 200 rpm, and experiments were performed at the temperature of 25 ± 1 °C (except for thermodynamic investigations with temperature variation). Full experimental conditions are systematically reported in the caption of the figures or tables. At the end of the experiments, a magnetic separation step allowed recovering spent sorbent particles and the residual concentration of uranium in the solution (C_{eq}, mg U L^{-1}) was assed using the Arsenazo III spectrophotometric method (Marczenko, 1976). The mass balance equation served for determining the amount of metal bound to the sorbent (q, mg U g^{-1}):

$$q_{eq} = (C_0 - C_{eq}) \times V/m \quad (1)$$

The distribution coefficient K_d is obtained by the q_{eq}/C_{eq} ratio and Eq. (2):

$$K_d = \left[(C_0 - C_{eq})/C_{eq}\right] \times V/m \quad (2)$$

Uptake kinetics was obtained by similar procedure, at given contact times samples were collected, magnetically separated and the residual concentration in the substrate was determined by spectrophotometry. The samples (max 5 mL volume) were collected with a syringe and a Nd-magnet was used for separating the solid from the liquid. The strength of the super-magnets and the small amount of sorbent make the separation instantaneous.

To evaluate the reusability of the sorbent, U(VI) sorption and desorption efficiencies were evaluated along 5/6 consecutive sorption–

desorption cycles. Experimental conditions for sorption corresponded to: (a) contact of 50 mg of sorbent with 50 mL of a U(VI) solution (C_0: 250 mg U L^{-1}) for 45 min under agitation in a closed flask, followed by (b) magnetic separation, and (c) spectrophotometric analysis of residual uranium concentration. The sorbent was rinsed with demineralized water before processing metal desorption. U(VI) desorption was operated at room temperature by contact of the collected sample with 50 mL of a urea solution (0.5 M, at slightly acidic pH; i.e., close to 2–3). After magnetic separation, uranium concentration in the eluate was analyzed and the mass balance equation was used to evaluate the desorption efficiency.

3. Results and discussion

3.1. Characterization of sorbents - summary

The relative fraction of magnetite in the hybrid materials was determined by weight loss at 500 °C. Whatever the sorbent, the fraction of magnetic core represented about 47–53% of total weight. This information is quite important for the discussion of sorption performance since half of the total weight of the sorbents is represented by the inorganic fraction that has less affinity for uranyl ions than chitosan derivatives. In the comparison of sorption properties of hybrid materials to raw chitosan or pure chitosan derivatives this relative fraction should be taken into account.

Table 1 reports the main physico-chemical characteristics of these hybrid materials. Element analysis confirms the efficient grafting of substituents on chitosan backbone. Indeed, the mass percentage of nitrogen increases from 1.7% to 3.1–4.8% (depending on the chemical grafting). It is noteworthy that the increase in nitrogen content does not necessarily mean that the amine groups are available and accessible for interacting with uranyl ions (UO_2^{2+}, or hydrolyzed species). In the case of DETA grafting on chitosan magnetic nano-based particles the grafting yield of DETA on nitrogen in the cross-linked chitosan was evaluated to 90% taking into account (a) the actual organic fraction, and (b) the increase in nitrogen percentage on this actual organic phase of the materials DETA-grafted and raw crosslinked chitosan magnetite hybrid: the increase in nitrogen content (i.e., 2.83 times) is consistent with the suggested structure of the derivative (Fig. S1, see Supplementary information). In the case of cysteine derivative the presence of S element also confirms the successful grafting of the amino-acid. The reactivity of these new functional groups depends on the mode of grafting and the accessibility and availability of amine and sulfur groups. FT-IR spectrometry was used for characterizing the gradual chemical modification of chitosan along the synthesis procedure. The grafting of the epichlorohydrin (for biopolymer cross-linking and for inserting anchoring arms for the immobilization of amino-acids or DETA) was identified by the appearance of a specific band (at 792 cm^{-1}: -CH_2-Cl band); this bands progressively disappeared with immobilization of the substituent (accompanied by the release of chlorine). The immobilization of the substituents was also demonstrated by the increase of the typical amine (or amide band) (Galhoum et al., 2015c; Mahfouz et al., 2015) and COO^- bands (around 1640 cm^{-1}) (Galhoum et al., 2015a, 2015d). The presence of magnetite was also identified by the appearance of a band close to 568 cm^{-1}: this is generally attributed to the Fe-O stretching vibration in Fe_3O_4 (Galhoum et al., 2015c).

Table 1 also reports the magnetization saturation (Ms) of hybrid materials: it varies between 10 and 23 emu g^{-1}, according the ranking: cysteine > DETA >> serine > alanine. This is 3 to 4 times less than the values found in the literature for pure magnetite nanoparticles (Wang et al., 2013). The decrease in Ms. may be explained by several reasons including: (a) the fact that about 50% of the mass of the hybrid material is constituted by an organic coating with no magnetic properties; and (b) the formation of a layer at the surface of nano-objects also contributes to reduce the magnetization moment of the magnetic core (Bhatt et al., 2010). It is noteworthy that the hysteresis loops (not shown) did not show coercivity or remanence (Galhoum et al., 2015a, 2015c): this means that all these materials are super-paramagnetic. This super-paramagnetism is frequently associated to nanometric-size magnetic objects; the limit size for observing this effect is generally considered close to 25 nm (Cao et al., 2014). This super-paramagnetism means that the nanoparticles will be readily recovered by external magnetic field.

XRD analysis confirmed the presence of magnetite with the characteristic peaks corresponding to indices (111), (220), (311), (400), (422), (511), (440) close to $2\theta = 20°, 30°, 36°, 43°, 54°, 57°$ and 63°, respectively (Galhoum et al., 2015d; Mahfouz et al., 2015). This is representative of the spinel Fe_3O_4 structure, characterized by high magnetic properties (Wang et al., 2011). It is noteworthy that the XRD patterns were not well resolved; this may be explained by the effect of coating the magnetite nanoparticles with the polymer layer. The Scherrer equation was applied to the band corresponding to (311) index (the largest band). The full-width at half maximum intensity (FWHM) was determined and the size of crystals was deduced (Table 1). DETA sorbent exhibited much smaller particles (around 6.5 nm) compared to amino-acid derivatives (crystal size ranged between 11.6 and 13.5 nm). These sizes are systematically below the limit size (25 nm) reported for enhanced superparamagnetic character.

TEM observation confirmed the nano-size of sorbent particles. The size and morphology of the particles was roughly homogeneous: globular particles of size ranging between 15 and 40 nm for amino-acid derivatives, and slightly less (between 10 and 30 nm) for DETA-derivative (Galhoum et al., 2015a, 2015c). This means that the organic-coated magnetite particles tend to aggregate due to dipole-dipole interactions. Some larger agglomerates (around 200–300 nm) can be also observed but under strong agitation they are readily dispersed. In any case, whatever the size of aggregates or agglomerates, the sorbent particles are sub-micron sized and fast sorption kinetics can be expected.

3.2. Sorption properties

3.2.1. pH selection

The sorption of metal ions is usually strongly affected by the pH due to several reasons associated to the proper chemistry of the sorbent (protonation/deprotonation, polymer conformation, polymer stability, etc.) and the speciation of metal ions (hydrolysis phenomena,

Table 1
Characterization of sorbents.

Sorbent	Element analysis				Titration analysis	VSM analysis	XRD analysis	TEM analysis
	C (%)	H (%)	N (%)[a]	S (%)	-NH_2 groups (mmol g^{-1})	Saturation magnetization (emu g^{-1})	Nanoparticle size (nm)[b]	Agglomerate size (nm)[c]
Magnetite/chitosan	14.2	2.6	1.7	–	2.86	–	–	
DETA	18.1	2.8	4.8	–	4.54	20.5	6.5	10–30
Alanine	17.2	2.7	3.5	–	3.94	14.0	13.0	15–40
Cysteine	19.8	3.9	3.1	2.3	3.54	21.5	13.5	15–40
Serine	16.2	2.6	3.3	–	3.60	10.6	11.6	15–40

[a] Amount of nitrogen per gram of sorbent (mmol N g^{-1}).
[b] Nanoparticle size determined by the Scherrer equation.
[c] Superstructure of larger size (up to 200–300 nm) were also formed but tended to disperse under strong agitation.

complexation with other compounds of the solution, etc.). Fig. 1a shows the impact of initial pH on sorption capacity; the four sorbents show a very similar trend: from pH 1 to pH 3.5 the sorption capacity linearly increased while above pH 3.5 and up to pH 5–5.8 the sorption capacity stabilized; above pH 5.8 the efficiency or uranyl removal tended to slightly increase again. The variation in recovery efficiency is relatively small but could be explained by the occurrence of precipitation phenomenon. Actually the pH significantly varied during the sorption step: Fig. S2 (see Supplementary information) shows that below pH 3 the pH tended to decrease, while above pH 3 and up to pH 6 the equilibrium pH value tended to increase. The highest pH variation was observed around pH 3.5, and DETA-derivative showed highest pH variations: this is probably due to the presence of 2 primary amine groups and a tertiary amine group (though the grafting of DETA on chitosan backbone via epichlorohydrin may affect the acid-base properties of one or more of these amine groups). The relatively stable pH range around pH 4.5 means that the materials have a kind of buffering effect in moderately acid solutions. It is noteworthy that pH slightly increased again above pH 6: this is probably due to the beginning of uranyl precipitation under the form of colloidal $UO_2(OH)_2$ species or solid precipitates (depending on metal concentration). In order to avoid these mechanisms of hydrolysis and precipitation (and subsequent misinterpretation of sorption capacities) experiments were not taken into account in the interpretation of pH effect for pH values higher than 5.8 and for further experiments. Actually the formation of polynuclear and polyhydrolyzed uranyl species is function of both pH and metal concentration (Guibal et al., 1992), at least below pH 5.8 with impact on pH variation and metal sorption; however, under selected experimental conditions, the precipitation of uranyl begins at pH close to 5.8.

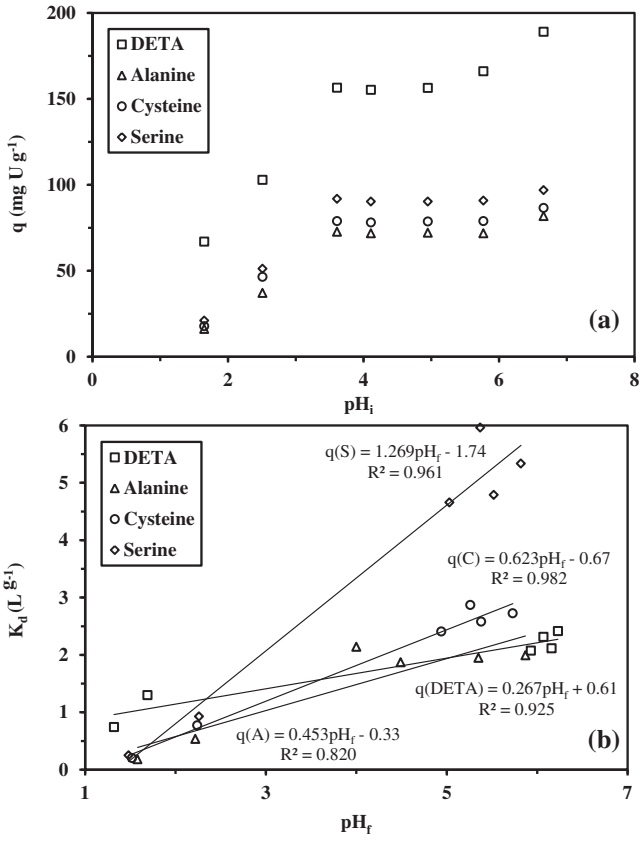

Fig. 1. Effect of pH on uranyl sorption using functionalized-chitosan magnetic nano-based particles: (a) sorption capacity as a function of initial pH; (b) distribution coefficient (K_d) as a function of equilibrium pH (C_0: 100 mg U L^{-1}; sorbent dosage, SD: 200 mg L^{-1}; agitation time: 2 h; agitation speed, v: 200 rpm; T: 25 °C).

The protonation of amine groups and carboxylic groups decreases with increasing the pH; this makes possible the binding of metal cations. Amino acids have carboxylic groups with pK_a in the range 1.9–2.4, while the pK_a of their amine groups vary between 9.15 and 9.69 (Table S1, see Supplementary information): this means that above pH 2–3 carboxylic groups are the main reactive groups for amino-acid derivatives. Their isoelectric points range between 5.07 and 6.0. In the case of DETA, the pK_as of amine groups stand between 4.34 and 9.94: obviously when the pH increases it enhances the binding properties for metal cations (UO_2^{2+}, and other cationic forms, such as $UO_2(OH)^+$, $(UO_2)_2(OH)_2^{2+}$, $(UO_2)_3(OH)_5^+$). In addition to these groups the proper amine groups of chitosan that were not involved in the grafting of substituents can bind uranyl species: the pK_a of amine groups in chitosan strongly depends on the degree of deacetylation of chitosan; however, its ranges between 6.3 and 6.7 for most common commercial samples (having degree of deacetylation in the range 80–95%). This means that sorption of uranyl ions on chitosan material will also be enhanced in neutral or moderately acid solutions. In the sorption of uranyl ions on *Mucor miehei* (a fungal biomass, whose cell wall is rich in chitosan) (Guibal et al., 1992), and chitosan a clear correlation was established between high sorption capacities and both the deprotonation of amine groups and the formation of polynuclear hydrolyzed species (Guibal et al., 1994). The highest sorption capacities (under selected experimental conditions) were obtained with DETA-derivative, probably due to the increased density of reactive groups (polyamine groups). Another mechanism that could be involved in metal binding in acidic solutions (lower values of selected pH range, which are less favorable for direct binding on free carboxylic acid and free amine groups) may consist in the binding of anionic species (formed in the presence of sulfate anions, such as $UO_2 \cdot (SO_4)_2^{2-}$ or $UO_2 \cdot (SO_4)_3^{4-}$) onto protonated amine groups.

Fig. 1b shows the rough correlation existing between the equilibrium pH and the distribution coefficients (i.e., $K_d = q / C_{eq}$, L g^{-1}) for the different sorbents (data corresponding to the precipitation of uranyl ions have been removed for calculating the correlation coefficients). Substantial differences are observed in their slope analysis. The plot of log K_d vs log H_3O^+ is frequently used in solvent extraction system and resin systems for evaluating the stoichiometry of proton/metal exchange. Fig. S3 (see Supplementary section) shows the two sections-plots: a first initial increasing section (with a slope ranging between 0.65 and 0.80) followed by a quasi-constant section (above pH 3–3.5).

Apart the problems of uranyl precipitation that may occur at pH higher than 6, it is also important to take into account the partial dissolving of magnetite particles when the pH decreases below pH 1.6. For all these reasons and based on Fig. 1 further experiments have been performed at pH 4.

3.2.2. Sorption isotherms and thermodynamic parameters

Uranium sorption isotherms were determined at pH 4 for the four sorbents (Fig. 2): the sorption capacity is represented as a function of residual metal concentration to illustrate the distribution of metal ions between the liquid and solid phases, at equilibrium. The curves are following the same trend: a sharp initial section with strongly increasing sorption capacity (residual concentration range: 0–25 mg U L^{-1}) followed by a progressive increase in the sorption capacity (residual concentration range: 25–120 mg U L^{-1}) and terminated by a saturation plateau.

Several models have been designed for describing sorption isotherms (Tien, 1994). The Langmuir and the Freundlich models are the most frequently used. The Freundlich model is a power-type function which is obviously inappropriate for describing the asymptotic trend observed for sorption isotherms in Fig. 2. The Langmuir equation, which is described by Eq. (3), is more appropriate for fitting isotherms. In Fig. 2 the solid lines represent the fitted curves with the Langmuir

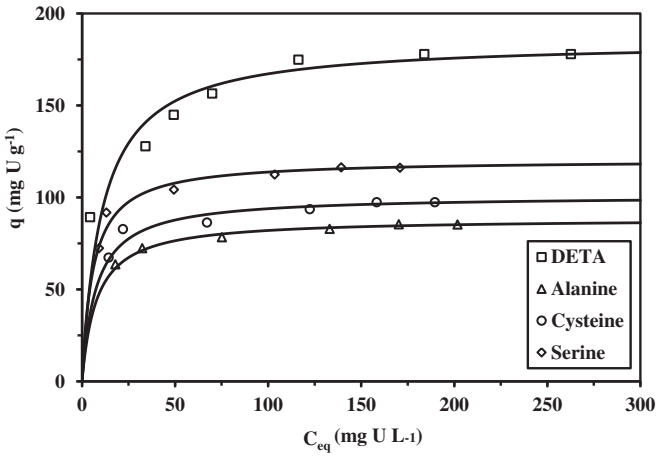

Fig. 2. Uranyl sorption isotherms using functionalized-chitosan magnetic nano-based particles (pH 4) (solid lines: fit of experimental data with Langmuir model using parameters from Table 2).

parameters reported on Table 2:

$$q = \frac{q_m \times b \times C_{eq}}{1 + b \times C_{eq}} \quad (3)$$

where q_m (mg U g^{-1}) is the maximum sorption capacity at saturation of the monolayer, b (L mg^{-1}) is the affinity coefficient.

The sorbents can be ranked according: DETA > Serine > Cysteine > Alanine in terms of maximum sorption capacities. A linear trend is obtained when correlating maximum sorption capacity to nitrogen content for DETA, serine and cysteine derivatives (Table 2), while alanine derivative leaves this trend. This can probably be explained by the fact that the supplementary amine group brought by alanine grafting is involved in the linking of the amino-acid (Fig. S1, see Supplementary information): this reactive groups are less accessible and available for metal binding than free amine groups as in DETA, serine and cysteine derivatives. The maximum sorption capacities in molar units range between 0.37 and 0.78 mmol U g^{-1} sorbent. This is much less than the proportion of amine groups in the sorbents; this also means that all reactive groups are probably not accessible or available (involved in grafting, etc.). Based on the fact that about 50% of the mass of the sorbents is constituted of magnetic core (with very limited sorption capacity for uranium (Das et al., 2010)), the sorption capacities of organic phase of the sorbents range between 0.74 and 1.56 mmol U g^{-1} 1 organic fraction.

On the opposite hand, considering the affinity coefficient (i.e., b) the sorbents can be ranked according: Serine > Cysteine ≈ Alanine > DETA. The term $q_m \times b$ represents the initial slope of the sorption isotherm; this is analogous in dimensional terms to a distribution coefficient (K_d, L g^{-1}). The sorbents can be ranked according Serine > DETA > Cysteine > Alanine. Globally, the serine and DETA derivatives show the best sorption performance compared to the other sorbents probably due to the availability and accessibility of their carboxylic groups and/or amine groups. DETA only holds amino groups (primary and secondary) while for serine terminating end holds both secondary amino group and carboxylic group (in addition to the secondary amino group from chitosan on which the amino-acid is grafted). Cysteine also holds secondary amino group and carboxylic group in a configuration close to that of serine; the additional sulfur bond involved in the grafting mechanism is probably poorly reactive. No clear explanation is available for explaining the highest efficiency of serine over cysteine. The weakest sorption activity of alanine-based sorbent is probably associated to the absence of free amino group at the terminating end of the polymer: the decrease in the density of sorption sites may explain the lower sorption capacity. In addition, in the case of DETA the long chain (with highest mobility and ability to adopt a more favorable configuration to bind uranyl cations) may explain the good sorption properties of this derivative.

The thermodynamics of uranium sorption using these sorbents were calculated based on the affinity coefficients determined from sorption isotherms at different temperatures, or from the distribution coefficients (Galhoum et al., 2015d, 2015e; Mahfouz et al., 2015) and the usual equations Eqs. (4)–(5):

$$\Delta G^0 = -RT \ln K_d \quad \text{or} \quad \Delta G^0 = -RT \ln b \quad (4)$$

$$\Delta G^0 = \Delta H^0 - T\Delta S^0 \quad (5)$$

Table 3 reports the thermodynamic constants of the different systems. Though they are slightly different for the four sorbents they remain in the same order of magnitude and follow the same trends:

(a) Exothermic sorption (negative value of ΔH^0),
(b) Spontaneous sorption (negative value of ΔG^0),
(c) Entropic control on sorption mechanism (regardless of temperature, $|\Delta H^0| < |T\Delta S^0|$),
(d) Increased randomness of the system after metal sorption (positive value of ΔS^0),

The comparison of maximum sorption capacities with enthalpy showed that the sorption increased with the absolute value of the enthalpy and decreased with decreasing the value of entropy: almost linearly for amino-acid derivatives while DETA derivative displayed a distinct trend (probably due to different density of sorption sites and to different reactive groups: no carboxylic groups, contrary to amino-acid derivatives).

Table 4 reports the main U(VI) sorption properties of a series of sorbents. Though some sorbents show much higher maximum sorption capacities than the sorbents developed in this study, DETA-functionalized chitosan magnetic nano-based particles appear to be promising based also on their fast uptake kinetics.

3.2.3. Uptake kinetics and mass transfer characteristics

The design of a sorbent requires taking into account uptake kinetics to (a) define the minimum contact time, (b) identify the controlling steps (including more specifically the mass transfer steps), and (c) optimize the design of sorbent material. The sorption of target solute onto a sorbent involves different mechanisms and different steps including the proper reaction rate but also diffusion mechanisms (bulk diffusion, film diffusion, intraparticle diffusion) (Tien, 1994). As already reported in

Table 2
Parameters of the Langmuir equation for the sorption of uranyl ions using functionalized-chitosan magnetic nano-based particles (at pH 4).

Sorbent	q_m (mg U g^{-1})	b (L mg^{-1})	$q_m \times b$ (L g^{-1})	R^2
DETA	185.2	0.093	17.2	0.998
Alanine	88.5	0.127	11.2	0.999
Cysteine	101.0	0.132	13.3	0.999
Serine	120.5	0.170	20.5	0.999

Table 3
Thermodynamic parameters obtained using the affinity coefficients of the Langmuir equation for the different sorbents and varying temperature (in the range 20–40 °C).

Sorbent	ΔH^0 (kJ mol^{-1})	ΔG^0 (kJ mol^{-1})	ΔS^0 (J mol^{-1} K^{-1})
DETA	-12.4	-30.8/−32.3	62.0
Alanine	-10.0	-29.0/−30.6	64.0
Cysteine	-11.8	-29.5/−31.0	59.0
Serine	-9.5	-32.9/−34.0	70.0

Table 4
Uranium sorption performances using different sorbents.

Sorbent	pH	q_m (mg U g^{-1})	b (L mg^{-1})	Equilibrium time (min)	PSORE rate constant (g mg^{-1} min^{-1})	Reference
PVA/CNT and derivatives	3	122–233	0.0024–0.0055	120	–	Abdeen and Akl (2015)
Ca-alginate beads	5	24	0.03	80	0.0068	Bai et al. (2013)
HDTMA modified tuff	4	51	0.023	100	0.0030	Bampaiti et al. (2015)
Phosphorus-modified resin	5	89	0.035	150	0.0228	Cao et al. (2013)
Functionalized mesoporous carbon	4	97	0.122	15	0.0082	Lin et al. (2013)
Bifunctional amidoxime resin	7	169	1.51	–	0.033	Wei et al. (2015)
Ion-imprinted magnetic chitosan resin	5	187	0.0088	60	0.0014	Zhou et al. (2012)
LDH-C-magnetic sorbent	6	227	0.09	100	0.0014	Zhang et al. (2013)
Functionalized poly(acrylonitrile) fibers	4	248	0.010	2–3	–	Chanda and Rempel (2003)
Magnetite particles	7	5	–	4	–	Das et al. (2010)
TEPA modified glycidyl methacrylate magnetic resin	4.5	409	0.00084	60	0.0008	Donia et al. (2009)
TEPA modified chitosan magnetic resin	4	397	0.0082	30	0.0006	Elwakeel et al. (2014)
DETA-chitosan magnetic nano-based particles	4	185	0.093	40	0.0037	Mahfouz et al. (2015)
Alanine-chitosan magnetic nano-based particles	4	88	0.127	60	0.0019	Galhoum et al. (2015d)
Cysteine-chitosan magnetic nano-based particles	4	101	0.132	60	0.0031	Galhoum et al. (2015e)
Serine-chitosan magnetic nano-based particles	4	120	0.170	60	0.0022	Galhoum et al. (2015d)

HDTMA: hexadecyl-trimethylammonium; LDH: Ni-Al layered double hydroxide deposited on carbon-coated magnetite nanoparticles.

the introduction, for justifying the synthesis of nano-based particles, the sorption properties of chitosan (and derivatives) are generally controlled (in terms of kinetics) by the resistance to intraparticle diffusion. The objective of designing magnetic nano-based particles consisted in reducing the contribution of resistance to intraparticle diffusion (small-size particles) and enhancing the solid/liquid separation properties (magnetic properties). Uptake kinetics were carried out and Fig. 3 compares the kinetic profiles for the four sorbents under similar experimental conditions. As expected the uptake kinetics were quite fast: the equilibrium was reached within 40–60 min. About 50% of total sorption occurs within the first five minutes of contact, while >90% of total sorption occurred within 45 min. With conventional powder/grain form, chitosan (and derivatives) usually requires several hours (and even several days) for reaching the equilibrium. This improvement clearly justifies the physical modification of the material. Both the small size of the particles, the thin coating of polymer-based sorbent on magnetic core contribute to limit the effect of resistance to intraparticle diffusion. Several simple models have been tested for fitting experimental kinetic curves (Galhoum et al., 2015d, 2015e; Mahfouz et al., 2015), including the Weber & Morris model (simplified approach of resistance to intraparticle diffusion, Weber and Morris, 1963), the pseudo-first order reaction equation (PFORE) and the pseudo-second order reaction equation (PSORE) (Ho and McKay, 1999). Best fit of experimental data were systematically obtained using the PSORE (Eqs. (6a) to (6c)):

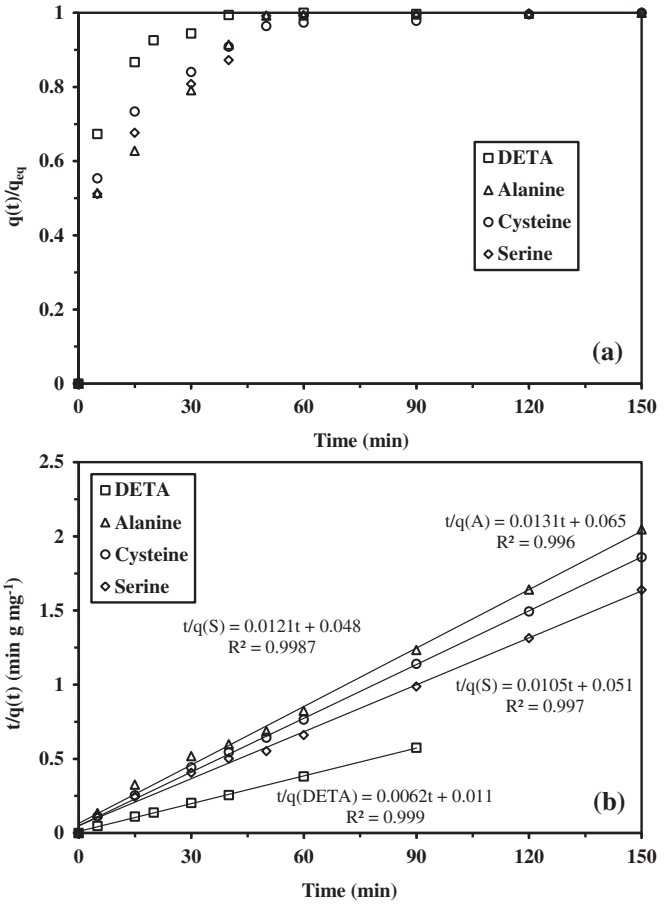

Fig. 3. Uranium uptake kinetics using functionalized-chitosan magnetic nano-based particles: (a) fractional approach to equilibrium ($q(t)/q_{eq}$); (b) fit of experimental curves with the pseudo-second order rate equation and parameters from Table 3 (C_0: 110 mg U L^{-1}; pH ≈ 4; SD: 1 g L^{-1} (except for DETA: 200 mg L^{-1}); T: 25 °C).

$$\frac{dq(t)}{dt} = k_2\left(q_{eq} - q(t)\right)^2 \tag{6a}$$

$$q(t) = \frac{k_2\ q_{eq}^2\ t}{1 + k_2\ q_{eq}\ t} \tag{6b}$$

$$\frac{t}{q(t)} = \frac{1}{k_2 q_{eq}^2} + \frac{1}{q_{eq}}t \tag{6c}$$

where k_2 is the apparent pseudo-second order reaction rate (g mg^{-1} min^{-1}), q_{eq} is the equilibrium sorption capacity (mg U g^{-1}). Table 5 reports the parameters of the PSORE for the different systems: the sorption capacity at equilibrium was systematically overestimated with the model while the rate constants were in the same range of magnitude ($1.94 \cdot 10^{-3}$–$3.66 \cdot 10^{-3}$ g mg^{-1} min^{-1}). Table 4 reported the

Table 5
Kinetic parameters for uranium sorption using functionalized-chitosan magnetic nano-based particles.

Sorbent	$q_{m,exp.}$ (mg U g^{-1})	$q_{m,PSORE}$ (mg U g^{-1})	$k_2 \times 10^3$ (g mg^{-1} min^{-1})	R^2
DETA	157.3	161.3	3.66	0.999
Alanine	73.3	77.5	1.94	0.997
Cysteine	80.7	82.6	3.11	0.999
Serine	91.6	95.2	2.19	0.997

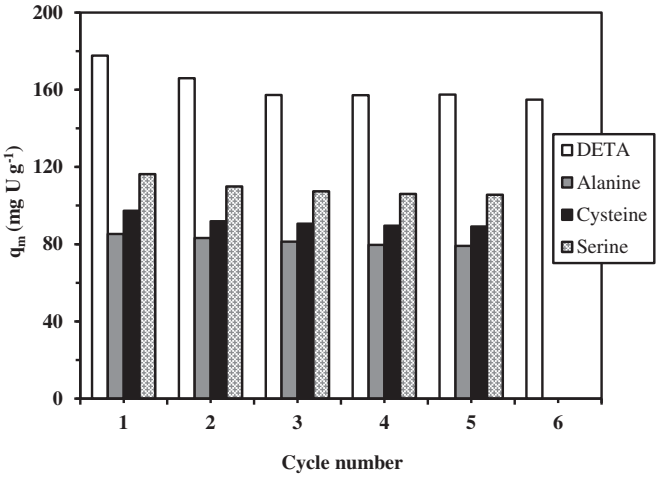

Fig. 4. Recycling of sorbents for uranium sorption using functionalized-chitosan magnetic nano-based particles (Sorption: SD: 200 mg L^{-1}; C_0: 200 mg U L^{-1}; pH 4; T: 25 °C; contact time: 40 min - Desorption: 0.5 M urea acidic solution (pH 2); SD: 4 g L^{-1}; T: 25 °C; contact time: 30 min).

kinetic parameters for a series of sorbents; except for chemically modified polyacrylonitrile fibers (for which equilibrium time was very short; i.e.; 2–3 min (Chanda and Rempel, 2003)) the equilibrium times reported for the present sorbents are among the shortest. The strict comparison of reaction rates is obviously made difficult by the diversity in experimental conditions (sorbent dosage, metal concentration, etc.) but these sorbents appear to offer a good compromise between kinetic and equilibrium performances. In terms of kinetic rates the sorbents can be ranked according: DETA > Cysteine > Serine ≈ Alanine, consistently with the general shape of the fractional approach to equilibrium (Fig. 3a).

3.2.4. Uranium desorption and sorbent recycling

The most sophisticated are the sorbents (as the result of more or less complex modification of raw materials) the most necessary is the recovery of metal and the recycling of the sorbent for making the process competitive. Usually the recovery of uranium from chitosan-based sorbents is carried out using acidic solutions (Elwakeel et al., 2014; Schleuter et al., 2013) or sodium bicarbonate solutions (Jansson Charrier et al., 1996; Oyola et al., 2016; Tan et al., 2015). In the present studies acidic urea solutions (0.5 M in slightly acidic solutions; pH > 2) were used for comparing sorption performance along 5 to 6 sorption/desorption cycles. Excessive acidic conditions may lead to instability of magnetic core a pH higher to 3 was preferred to prevent the partial dissolving of iron oxide fraction in the composite material. This sounds to be a good compromise; although bicarbonate solutions would probably constitute an efficient alternative. Fig. 4 reports the evolution of the sorption capacity for 5 or 6 cycles: a slight and progressive decrease is observed; however, at the last cycle, the loss of sorption capacity did not exceed 13% for DETA (average value 162 ± 8 mg U g^{-1}), 7% for alanine (82 ± 2 mg U g^{-1}), 8% for cysteine (92 ± 3 mg U g^{-1}) and 9% for serine (109 ± 4 mg U g^{-1}). These results mean that, indifferently to the compound grafted on chitosan/magnetite hybrid material, the sorbents are remarkably stable in their sorption performance for at least 5 cycles of sorption/desorption.

4. Conclusion

The immobilization of chitosan on a magnetic core (by a simultaneous precipitation of chitosan and synthesis of iron oxide, through a combination of hydrothermal treatment and precipitation process) allows preparing nano-based particles with super paramagnetic properties. Sorbent particles can be very efficiently recovered by external magnetic field. Despite their tendency to agglomerate the aggregate remain at a nano-scale; as a consequence the thin layer of biopolymer, which was modified by grafting a series of amino-acids and diethylenetriamine, may reduce the impact of resistance to intraparticle diffusion in the control of uptake kinetics. This is confirmed by the fast kinetics (which takes about 40–60 min to reach the equilibrium): pseudo-second order rate equation fits well kinetic profiles. Sorption isotherms are perfectly described by the Langmuir equation and thermodynamic parameters show that the reaction is endothermic, spontaneous and controlled by entropy (increased randomness during uranyl sorption). The metal can be readily desorbed using acidic solution containing 0.5 M urea. The desorption of uranyl ions and the recycling of the sorbent over 5/6 cycles showed that the sorbents can be reused for a minimum of 5 cycles with a low decrease in sorption capacity that does not exceed 9%. Comparing both maximum sorption capacity (equilibrium) and equilibrium time or kinetic rate allows ranking the sorbents according the sequence: DETA > Serine > Cysteine > Alanine.

DETA-derivative of chitosan, immobilized on magnetic nano-based particles, appears to be very efficient and promising for the fast recovery of uranyl ions. The magnetic properties allow using the material in hazardous environment with enhanced mass transfer characteristics and high sorption capacities.

Acknowledgements

Authors acknowledge the financial support from French Government (A.A.G. research fellowship from Institut Français d'Egypte). Authors acknowledge the technical and scientific support of Prof. Sayed T Abdel-Rehem (Ain Shams University, Egypt) and Prof. Atem A Atia (Menoufia University).

References

Abdeen, Z., Akl, Z.F., 2015. Uranium(VI) adsorption from aqueous solutions using poly(vinyl alcohol)/carbon nanotube composites. RSC Adv. 5 (91), 74220–74229.
Bai, J., Fan, F., Wu, X., Tian, W., Zhao, L., Yin, X., Fan, F., Li, Z., Tian, L., Wang, Y., Qin, Z., Guo, J., 2013. Equilibrium, kinetic and thermodynamic studies of uranium biosorption by calcium alginate beads. J. Environ. Radioact. 126, 226–231.
Bampaiti, A., Misaelides, P., Noli, F., 2015. Uranium removal from aqueous solutions using a raw and HDTMA-modified phillipsite-bearing tuff. J. Radioanal. Nucl. Chem. 303 (3), 2233–2241.
Bhatt, A.S., Krishna Bhat, D., Santosh, M.S., 2010. Electrical and magnetic properties of chitosan-magnetite nanocomposites. Physica B 405 (8), 2078–2082.
Cao, Q., Liu, Y., Kong, X., Zhou, L., Guo, H., 2013. Synthesis of phosphorus-modified poly(-styrene-co-divinylbenzene) chelating resin and its adsorption properties of uranium(VI). J. Radioanal. Nucl. Chem. 298 (2), 1137–1147.
Cao, C., Xiao, L., Chen, C., Shi, X., Cao, Q., Gao, L., 2014. In situ preparation of magnetic Fe_3O_4/chitosan nanoparticles via a novel reduction–precipitation method and their application in adsorption of reactive azo dye. Powder Technol. 260, 90–97.
Chanda, M., Rempel, G.L., 2003. A superfast sorbent based on textile-grade poly(acrylonitrile) fiber/fabric. Rapid removal of uranium from mildly acidic aqueous solutions of low concentration. Ind. Eng. Chem. Res. 42 (22), 5647–5655.
Chen, X.T., He, L.F., Liu, R.Z., Zhang, C., Liu, B., Tang, Y.P., 2015. Effective uranium(VI) sorption from alkaline media using bi-functionalized silica-coated magnetic nanoparticles. RSC Adv. 5 (70), 56658–56665.
Das, D., Sureshkumar, M.K., Koley, S., Mithal, N., Pillai, C.G.S., 2010. Sorption of uranium on magnetite nanoparticles. J. Radioanal. Nucl. Chem. 285 (3), 447–454.
Donia, A.M., Atia, A.A., Moussa, E.M.M., El-Sherif, A.M., El-Magied, M.O.A., 2009. Removal of uranium(VI) from aqueous solutions using glycidyl methacrylate chelating resins. Hydrometallurgy 95 (3–4), 183–189.
Elwakeel, K.Z., Atia, A.A., 2014. Uptake of U(VI) from aqueous media by magnetic Schiff's base chitosan composite. J. Clean. Prod. 70, 292–302.
Elwakeel, K.Z., Atia, A.A., Guibal, E., 2014. Fast removal of uranium from aqueous solutions using tetraethylenepentamine modified magnetic chitosan resin. Bioresour. Technol. 160, 107–114.
Galhoum, A.A., Atia, A.A., Mahfouz, M.G., Abdel-Rehem, S.T., Gomaa, N.A., Vincent, T., Guibal, E., 2015a. Dy(III) recovery from dilute solutions using magnetic-chitosan nano-based particles grafted with amino acids. J. Mater. Sci. 50 (7), 2832–2848.

Galhoum, A.A., Mafhouz, M.G., Abdel-Rehem, S.T., Gomaa, N.A., Atia, A.A., Vincent, T., Guibal, E., 2015b. Cysteine-functionalized chitosan magnetic nano-based particles for the recovery of light and heavy rare earth metals: uptake kinetics and sorption isotherms. Nanomaterials 5 (1), 154–179.
Galhoum, A.A., Mahfouz, M.G., Abdel-Rehem, S.T., Gomaa, N.A., Atia, A.A., Vincent, T., Guibal, E., 2015c. Diethylenetriamine-functionalized chitosan magnetic nano-based particles for the sorption of rare earth metal ions Nd(III), Dy(III) and Yb(III). Cellulose 22 (4), 2589–2605.
Galhoum, A.A., Mahfouz, M.G., Atia, A.A., Abdel-Rehem, S.T., Gomaa, N.A., Vincent, T., Guibal, E., 2015d. Amino acid functionalized chitosan magnetic nanobased particles for uranyl sorption. Ind. Eng. Chem. Res. 54 (49), 12374–12385.
Galhoum, A.A., Mahfouz, M.G., Gomaa, N.A., Abdel-Rehem, S.S., Atia, A.A., Vincent, T., Guibal, E., 2015e. Cysteine-functionalized chitosan magnetic nano-based particles for the recovery of uranium(VI): uptake kinetics and sorption isotherms. Sep. Sci. Technol. 50 (18), 2776–2789.
Guibal, E., 2004. Interactions of metal ions with chitosan-based sorbents: a review. Sep. Purif. Technol. 38 (1), 43–74.
Guibal, E., Roulph, C., Lecloirec, P., 1992. Uranium biosorption by a filamentous fungus *Mucor miehei*: pH effect on mechanisms and performances of uptake. Water Res. 26 (8), 1139–1145.
Guibal, E., Saucedo, I., Jansson Charrier, M., Delanghe, B., Lecloirec, P., 1994. Uranium and vanadium sorption by chitosan and derivatives. Water Sci. Technol. 30 (9), 183–190.
Guibal, E., Jansson Charrier, M., Saucedo, I., Lecloirec, P., 1995. Enhancement of metal-ion sorption performances of chitosan - effect of the structure on the diffusion properties. Langmuir 11 (2), 591–598.
Ho, Y.S., McKay, G., 1999. Pseudo-second order model for sorption processes. Process Biochem. 34 (5), 451–465.
Jansson Charrier, M., Guibal, E., Roussy, J., Surjous, R., LeCloirec, P., 1996. Dynamic removal of uranium by chitosan: influence of operating parameters. Water Sci. Technol. 34 (10), 169–177.
Lapidus, G.T., Doyle, F.M., 2015. Selective thorium and uranium extraction from monazite: II. Approaches to enhance the removal of radioactive contaminants. Hydrometallurgy 155, 161–167.
Lin, W., Carboni, M., Abney, C.W., Taylor-Pashow, K.M.L., Vivero-Escoto, J.L., 2013. Uranium sorption with functionalized mesoporous carbon materials. Ind. Eng. Chem. Res. 52 (43), 15187–15197.
Mahfouz, M.G., Galhoum, A.A., Gomaa, N.A., Abdel-Rehem, S.S., Atia, A.A., Vincent, T., Guibal, E., 2015. Uranium extraction using magnetic nano-based particles of diethylenetriamine-functionalized chitosan: equilibrium and kinetic studies. Chem. Eng. J. 262, 198–209.
Marczenko, Z., 1976. Spectrophotometric determination of elements. Ellis Horwood Series in Analytical Chemistry. Ellis Horwood, Chichester (U.K.) (643 pp.).
Massart, R., 1981. Preparation of aqueous magnetic liquids in alkaline and acidic media. IEEE Trans. Magn. 17 (2), 1247–1249.
Oyola, Y., Vukovic, S., Dai, S., 2016. Elution by Le Chatelier's principle for maximum recyclability of adsorbents: applied to polyacrylamidoxime adsorbents for extraction of uranium from seawater. Dalton Trans. 45 (20), 8532–8540.
Schleuter, D., Gunther, A., Paasch, S., Ehrlich, H., Kljajic, Z., Hanke, T., Bernhard, G., Brunner, E., 2013. Chitin-based renewable materials from marine sponges for uranium adsorption. Carbohydr. Polym. 92 (1), 712–718.
Tan, L., Wang, Y., Liu, Q., Wang, J., Jing, X., Liu, L., Liu, J., Song, D., 2015. Enhanced adsorption of uranium (VI) using a three-dimensional layered double hydroxide/graphene hybrid material. Chem. Eng. J. 259, 752–760.
Tien, C., 1994. Adsorption calculations and modeling. Butterworth-Heinemann Series in Chemical Engineering. Butterworth-Heinemann, Newton, MA (243 pp.).
Wang, J.-S., Peng, R.-T., Yang, J.-H., Liu, Y.-C., Hu, X.-J., 2011. Preparation of ethylenediamine-modified magnetic chitosan complex for adsorption of uranyl ions. Carbohydr. Polym. 84 (3), 1169–1175.
Wang, B., Wei, Q., Qu, S., 2013. Synthesis and characterization of uniform and crystalline magnetite nanoparticles via oxidation-precipitation and modified co-precipitation methods. Int. J. Electrochem. Sci. 8, 3786–3793.
Weber, W.J., Morris, J.C., 1963. Kinetics of adsorption on carbon from solutions. J. Sanit. Eng. Div. ASCE 89, 31–60.
Wei, Y., Qian, J., Huang, L., Hua, D., 2015. Bifunctional polymeric microspheres for efficient uranium sorption from aqueous solution: synergistic interaction of positive charge and amidoxime group. RSC Adv. 5 (79), 64286–64292.
Xu, J., Chen, M., Zhang, C., Yi, Z., 2013. Adsorption of uranium(VI) from aqueous solution by diethylenetriamine-functionalized magnetic chitosan. J. Radioanal. Nucl. Chem. 298 (2), 1375–1383.
Yang, G., Tang, L., Lei, X., Zeng, G., Cai, Y., Wei, X., Zhou, Y., Li, S., Fang, Y., Zhang, Y., 2014. Cd(II) removal from aqueous solution by adsorption on α-ketoglutaric acid-modified magnetic chitosan. Appl. Surf. Sci. 292, 710–716.
Zagorodnyaya, A.N., Abisheva, Z.S., Sharipova, A.S., Sadykanova, S.E., Bochevskaya, Y.G., Atanova, O.V., 2013. Sorption of rhenium and uranium by strong base anion exchange resin from solutions with different anion compositions. Hydrometallurgy 131, 127–132.
Zhang, X., Wang, J., Li, R., Dai, Q., Gao, R., Liu, Q., Zhang, M., 2013. Preparation of Fe_3O_4@C@ layered double hydroxide composite for magnetic separation of uranium. Ind. Eng. Chem. Res. 52 (30), 10152–10159.
Zhou, L., Shang, C., Liu, Z., Huang, G., Adesina, A.A., 2012. Selective adsorption of uranium(VI) from aqueous solutions using the ion-imprinted magnetic chitosan resins. J. Colloid Interface Sci. 366 (1), 165–172.
Zhou, Z., Lin, S., Yue, T., Lee, T.-C., 2014. Adsorption of food dyes from aqueous solution by glutaraldehyde cross-linked magnetic chitosan nanoparticles. J. Food Eng. 126, 133–141.